7 Tesla MR Imaging: Opportunities and Challenges

MRT bei 7 Tesla: Möglichkeiten und Herausforderungen

Authors L. Umutlu[2], M. E. Ladd[2], M. Forsting[1], T. Lauenstein[1]

Affiliations
[1] Institute for Diagnostic and Interventional Radiology, University Hospital Essen
[2] Erwin L. Hahn Institute for Magnetic Resonance Imaging, University Duisburg-Essen

Key words
- MR imaging
- technical aspects
- diagnostic radiology

Zusammenfassung

Die Steigerung der Magnetfeldstärke geht mit einer Reihe von potenziell vorteilhaften physikalischen Veränderungen einher, die zu einer verbesserten Diagnostik von Erkrankungen führen können. Mit der erfolgreichen Einführung der in vivo 7 Tesla Magnetresonanztomografie wurde der wissenschaftliche Fokus auf die Etablierung verschiedener neuro- und allgemeinradiologischer Anwendungsfelder gelegt. Diese Übersichtsarbeit gibt einen Überblick über den aktuellen Stand der 7 Tesla MRT, verbunden mit dem Ziel die Möglichkeiten und Grenzen der Ultrahochfeldbildgebung aufzuzeigen.

Abstract

The urge to increase magnetic field strength is driven by a number of potentially beneficial physical changes, possibly resulting in improved MR diagnostics. With the successful introduction of in-vivo ultra-high-field MR imaging, by means of 7 Tesla MRI, the focus of scientific research has been set on compiling different applications of brain and body imaging. This review presents an overview on the current status of 7 T MR imaging, investigating the opportunities as well as challenges associated with ultra-high-field MRI.

Citation Format:
- Umutlu L, Ladd ME, Forsting M et al. 7 Tesla MR Imaging: Opportunities and Challenges. Fortschr Röntgenstr 2014; 186: 121–129

Introduction

After the introduction of the first 8 Tesla magnet at the Ohio State University in the late 1990s, there has been a continuously increasing number of ultra-high-field (> 7 Tesla) unit installations worldwide (approximately 40 to date) [1 – 5]. The urge to increase magnetic field strength is driven by a number of associated changes of physical features. These changes may entail positive as well as disadvantageous effects, signifying opportunities as well as challenges for the implementation of ultra-high-field MRI. Changes of physical properties include higher signal-to-noise ratios, increasing sensitivity to magnetic susceptibility and chemical shift as well as changing tissue relaxation times [6]. Some changes in physical features bear the potential to impede imaging at higher magnetic field strengths such as the hindered maintenance of a homogeneous RF (B_1) field. Furthermore, the increased power deposition results in restrictions due to the Specific Absorption Rate (SAR) [7]. Key physical changes are described hereafter:

- **SNR.** One of the most desirable changes, bearing the potential to improve the diagnostic ability of MR imaging, is the associated gain in signal-to-noise ratio (SNR). In theory, SNR increases linearly with the field strength, with minor restrictions due to limiting alterations in relaxation times and total body heating [6]. The affiliated increase of SNR can be deployed in imaging at a higher spatial or temporal resolution, or enable an improvement of both in terms of imaging at a higher spatiotemporal resolution [8]. Hence, dynamic imaging such as perfusion analysis can be performed more accurately. In addition, anatomical structures can be displayed in more detail. This has been proven feasible and beneficial regarding improved diagnostic ability in numerous high-field studies so far [9 – 13].
- **Magnetic susceptibility.** The associated increase in sensitivity to magnetic susceptibility can be

received 3.9.2012
accepted 8.7.2013

Bibliography
DOI http://dx.doi.org/10.1055/s-0033-1350406
Published online: 30.8.2013
Fortschr Röntgenstr 2014; 186: 121–129 © Georg Thieme Verlag KG Stuttgart · New York · ISSN 1438-9029

Correspondence
Dr. Lale Umutlu
Institut für Diagnostische und Interventionelle Radiologie und Neuroradiologie,
Universitätsklinik Essen
Hufelandstr. 55
45122 Essen
Germany
Tel.: ++ 49/02 01/72 38 45 27
Fax: ++ 49/02 01/7 23 15 63
lale.umutlu@uk-essen.de

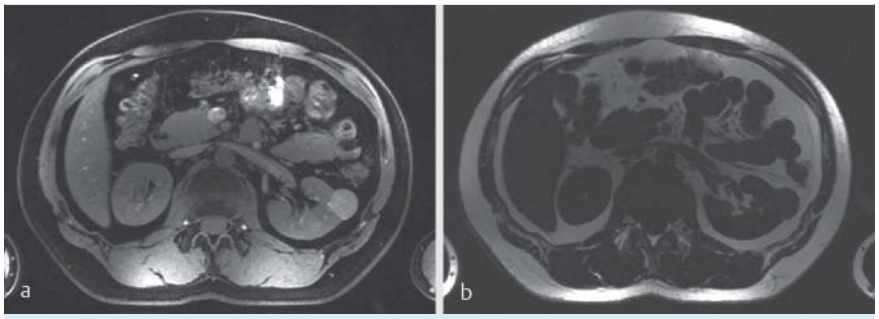

Fig. 1 **a** shows a fat-saturated 2 D FLASH image, **b** a concomitant water-saturated image of the abdomen, both acquired at 7 Tesla. Both images were acquired with TIAMO (Time-Interleaved Acquisition of Modes) showing excellent homogeneity of the imaged anatomy without B1 field inhomogeneities (Courtesy of Mr. St. Orzada Erwin L. Hahn Institute for Magnetic Resonance Imaging, University of Duisburg-Essen, Essen, Germany).

Abb. 1 **a, b** zeigen fett- **a** bzw. wassergesättigte **b** 2-D-FLASH-Bilder des Abdomen bei 7 Tesla. Beide Datensätze wurden mittels der TIAMO-Technik aufgenommen und sind durch ein homogenes B1-Feld ohne Signalvariationen gekennzeichnet.

positive as well as negative, depending on the particular application. With an increasing field strength, the RF field becomes more inhomogeneous and more susceptible to T2* dephasing effects, potentially improving the detection of blood products in brain MRI [12, 14] or impeding diagnostics, when imaging abdominal organs with air-tissue interfaces [6].

- **Chemical shift**. Increasing chemical shifting is another physical property that may be advantageous as well as disadvantageous for diagnostics. Chemical shift refers to the resonance frequency variations of different chemical species and can be classified as a chemical shift artifact of the first and the second kind. A chemical shift artifact of the first kind is caused by a difference between the resonance frequency of protons in water versus fat, leading to a misregistration artifact along the frequency-encoding axis and the section-selective dimension [6, 15 – 19]. It appears as a hypointense band toward the lower part and as a hyperintense band toward the higher part of the frequency-encoding gradient field. As the chemical shift artifact of the first kind is directly proportional to the strength of the magnetic field, the increase of the field strength has the potential for artifact exacerbation [6, 17, 19]. In contrast, the chemical shift artifact of the second kind does not increase with the magnetic field strength. Instead it is defined by the spatial resolution and is based on intravoxel phase cancellation effects in voxels comprising fat and water [6].
- **Tissue changes**. The diagnostic value of changes in T1 and T2 relaxation times at higher field strengths has not been fully exploited yet. T1 relaxation times are known to be prolonged at higher field strengths, leading to lower intrinsic soft tissue contrast. However, as the T1 time of paramagnetic agents such as gadolinium is shorter than that of soft tissue, contrast-enhanced tissue stands out markedly against surrounding tissue. Hence, diagnostic sensitivity is ameliorated by the enhanced contrast. This entails the potential for gadolinium dosage reduction while preserving diagnostic quality at higher field strengths [6, 20]. However, T2 effects are less predictable and may vary depending on the tissue with a slight overall decrease [7, 21].
- **SAR.** One of the most challenging factors of ultra-high-field imaging is related to the increased power deposition in human tissue, which is characterized by the Specific Absorption Rate (SAR) [6 – 8, 22, 23]. Energy deposition is known to increase with the square of the magnetic field [24]. Hence, the acquisition of RF-intense turbo-spin-echo (TSE) and fat-saturated sequences may be impaired in high-field MRI. Different techniques for mitigation may have to be applied at the cost of the SNR, including parallel imaging or flip angle modulation [22, 25].
- **B_1-field inhomogeneity.** RF inhomogeneities are known to entail severe impairment of image quality at ultra-high-field strength when imaging an FOV larger than circumscribed areas like the brain [26]. This is caused by the shortening of the wavelength, decreasing from 52 cm at 1.5 T to 12 cm at 7 T, which causes impeding standing waves or dielectric effects. Hence, RF shimming becomes crucial when a larger FOV is imaged [22, 24, 25, 27]. In an attempt to overcome impeding B_1 field inhomogeneities, different shimming techniques have been introduced for 7 Tesla body imaging. Specific circularly polarized modes have been applied for abdominal MRI [24, 25, 27] and individual RF mapping for female pelvis imaging [28] with successful reduction of impeding inhomogeneities and minor residual limitations. Orzada et al. proposed another dedicated shimming technique by the name of TIAMO (Time-Interleaved Acquisition of Modes) [29, 30]. This technique involves the acquisition of 2 time-interleaved images using different excitation modes to exploit the complementary RF patterns of the two modes to improve overall signal homogeneity [29, 30] (**Fig. 1**).

The objective of this article is to give an overview on current clinical applications of 7 Tesla MRI, utilizing the opportunities as well as coping with the challenges associated with ultra-high magnetic field strength.

Brain imaging

Initial studies on 7 Tesla brain MRI focused on the transformation of the increased SNR into high spatial resolution structural imaging. Thus highly-defined anatomical imaging of macro- and microstructures [14] as well superior assessment of disease becomes possible, e. g. in the case of neoplastic and inflammatory lesions at 7 T (e. g. multiple sclerosis) [9, 12] (**Fig. 2**). Besides structural imaging, first studies on 7 Tesla brain MRI disclosed an interesting characteristic of T1-weighted imaging at 7 T, by means of a homogeneously hyperintense delineation of arterial vasculature [31, 32]. The etiology of this feature is incompletely understood so far. Nevertheless, a combination of steady-state and inflow effects, as well as the application of local transmit/receive RF coils at 7 T, seems to be responsible [31, 33]. Grinstead et al. compared the signal intensity of arterial vasculature in MPRAGE (Magnetization Prepared Rapid Gradient Echo) imaging at 3 T and 7 T and confirmed the importance of local RF transmit coil systems at 7 T. According to their results, the utilization of local RF transmit coils at 7 T implies a non-selective inversion recovery pulse to effectively be a slab-selective IR pulse, resulting in high-signal intensity [33]. Furthermore, local RF transmit coils

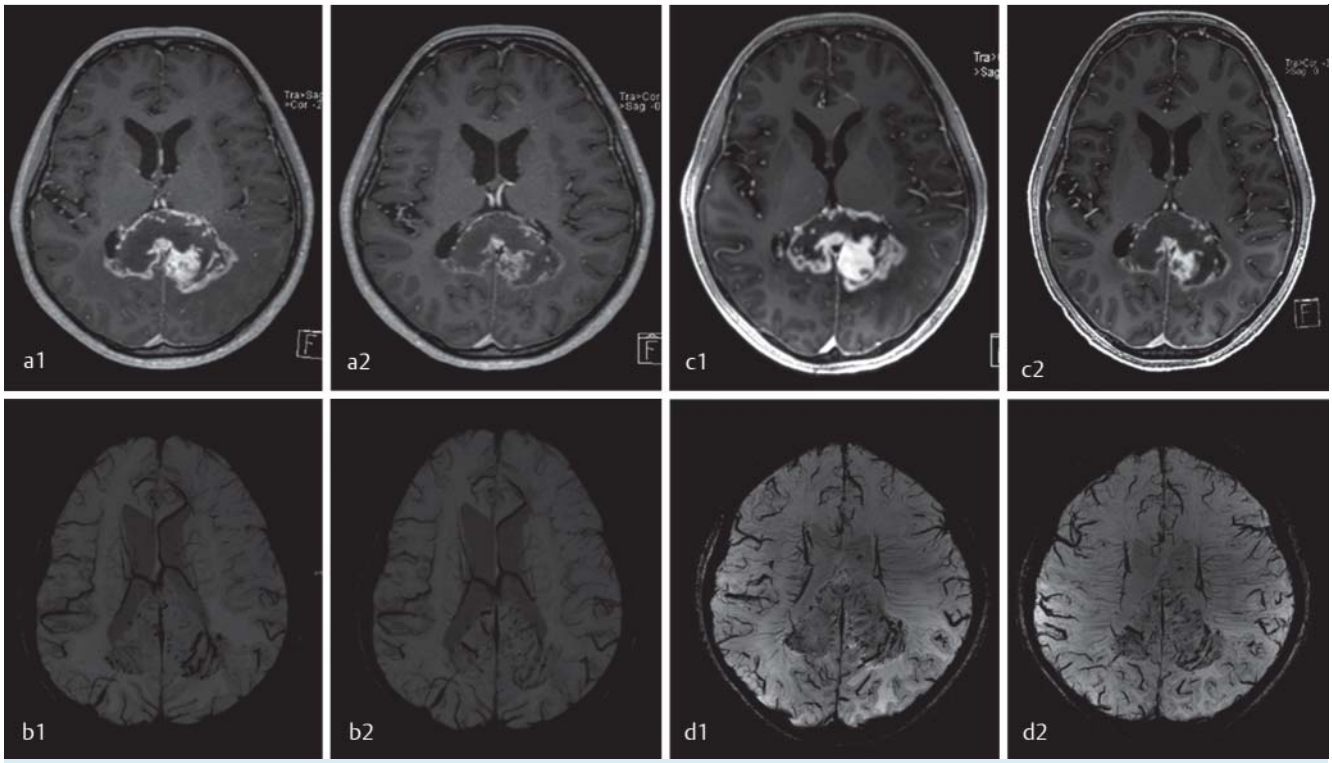

Fig. 2 Post-contrast MPRAGE **a**, **c** and SWI imaging **b**, **d** in a 54-year-old patient with glioblastoma multiforme under anti-angiogenetic chemotherapy. Figures a and b show 3 Tesla imaging, **c**, **d** concomitant 7 T images (pretherapeutic and follow-up after the first cycle of chemotherapy as designated in the images). Both field strengths offer excellent assessment of tumor delineation and size reduction in MPRAGE **a**, **c** imaging, with superior assessment of tumor microvasculature in 7 T MRI (d1, 2).

Abb. 2 Kontrastmittel-gestützte MPRAGE **a**, **c** und SWI Bildgebung **b**, **d** eines 54-jährigen Patienten mit einem Glioblastoma multiforme unter anti-angiogenetischer Chemotherapie. **a, b** zeigen 3 Tesla, **b, d** 7 Tesla Bilder der Tumormanifestation prätherapeutisch und unter Therapie (in Abbildung gekennzeichnet). Die MPRAGE Bildgebung zeigt eine äquivalente Diagnostik der Tumorgröße unter Therapie in beiden Feldstärken. 7 T SWI Bildgebung ermöglichte eine bessere Darstellung der Tumor-assoziierten Mikrovaskulatur.

excite a rather small RF volume where entering RF pulses are not pre-saturated, which potentially contributes to the hyperintense signal [34].

This interesting feature of T1-weighted MRI at 7 Tesla led to a shift of the focus of ultra-high-field brain imaging from structural to vessel diagnostics [10, 13, 31, 35, 36]. One of the first studies to assess the feasibility and diagnostic value of intracranial MRA at 7 Tesla was introduced by Maderwald et al. [31]. They compared the diagnostic ability of 3 D TOF MRA to non-enhanced VIBE (Volumetric Interpolated Breath-hold Examination) and non-enhanced MPRAGE imaging in 12 healthy volunteers as well as 13 patients. While the spatial resolution could be held equivalently high for all three sequences ($0.6 \times 0.5 \times 0.5 mm^3$), the acquisition time for TOF imaging was highest based on SAR constraints. In source imaging MPRAGE MRI was rated superior to the other sequences, as it provided the best delineation of arterial vasculature, and suffered least from intraluminal signal loss [31]. Mönninghoff et al. compared the diagnostic ability of 7 T versus 1.5 T time-of-flight (TOF) MRA in patients with intracranial aneurysms. They could prove a diagnostic benefit due to the increased spatial resolution of 7 T TOF MRA [10, 13]. After successful demonstration of the feasibility of 7 Tesla brain imaging, first field strength comparison trials were conducted (**Fig. 3**). Stamm et al. recently published their results on a comparison trial of TOF MRA and phase contrast MRA at 1.5, 3 and 7 Tesla. They could show the diagnostic equivalence of all three field strengths for the assessment of the large primary vessels of the Circle of Willis and an improved depiction of the first- and second-order branch arteries at 7 Tesla. Analysis of the SNR in the primary vessels revealed only a minor increase at 7 Tesla, mainly due to the acquisition of smaller voxel sizes [37].

Apart from vessel imaging, the increase of the field strength has also been demonstrated to be beneficial for functional MRI, based on the increased SNR and supralinear increase of BOLD (blood-oxygen-level-dependent) signal changes [38]. In an fMRI trial van der Zwaag et al. demonstrated a significant improvement of t-value and signal changes in the motor cortex with increasing field strength [39]. Recent studies on 7 T functional MRI showed its high diagnostic ability in stroke imaging and assessment of tissue viability due to the noninvasive quantification of intracellular sodium [40, 41].

Musculoskeletal imaging

As soon as 7 T MR imaging became bound to vendor-provided head coil systems, imaging of circumscribed anatomical areas small enough to fit into the coils, as in hand or ankle musculoskeletal (MSK) imaging, became a growing area of investigation. As MSK MRI involves imaging of stationary tissue without the need for breath-holding, potentially advantageous characteristics of high-field MRI could be exploited to their full extent. This results

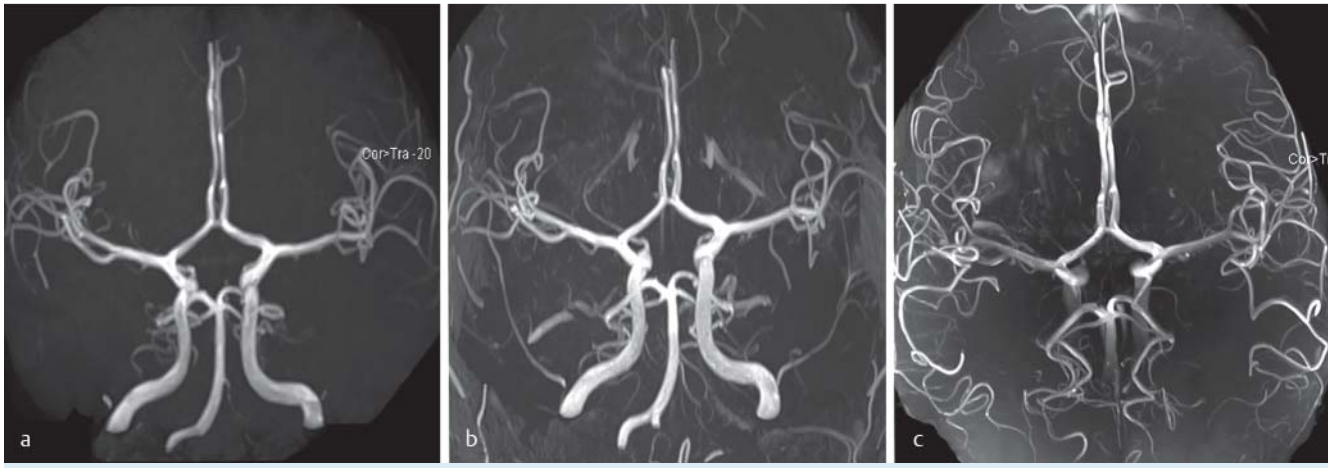

Fig. 3 TOF MRA at 1.5 T **a**, 3 T **b** and 7 T **c** demonstrating the improved delineation of peripheral vessel segments with increasing field strength.

Abb. 3 TOF MRA bei 1,5 T **a**, 3 T **b** und 7 T **c** zeigt eine verbesserte Darstellung kleiner peripherer Gefäßsegmente mit steigender Feldstärke.

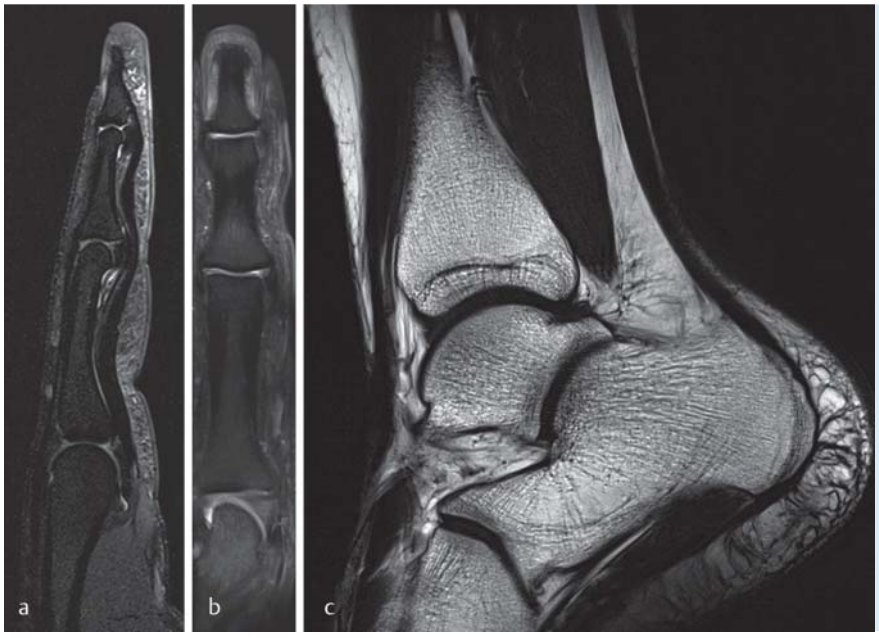

Fig. 4 **a, b** show 7 Tesla sagittal **a** and coronal **b** proton density weighted images with fat suppression of a finger, yielding detailed delineation of small finger joints and tendons. **c** shows 7 Tesla T1 TSE MRI of the ankle joint in sagittal view, providing high quality visualization of the trabecular bone within the tarsal bones with high spatial resolution (Courtesy of Prof. S. Trattnig, MR Centre-High Field MR, Department of Radiology, Medical University, Vienna, Austria).

Abb. 4 **a** (sagittal), **b** (koronar) zeigen eine detailreiche Darstellung der kleinen Gelenke und Sehnen eines Fingers in der fettgesättigten PD-T2-Sequenz bei 7 Tesla. **c** zeigt eine hochaufgelöste Abbildung des Sprunggelenkes in der T1 gewichteten TSE-Sequenz bei 7 Tesla.

in excellent visualization of detailed anatomy [42, 43] (▶ **Fig. 4**) and reveals its superiority compared to lower, yet well-established field strengths (3 T) [44, 45]. Juras et al. performed a comparison study of intraindividual imaging of the ankle at 7 T and 3 T. Their results demonstrated a significant increase in the SNR at 7 T for 3 D gradient echo (GRE) and 2 D TSE imaging of 60.9 % and 86.7 %, respectively. An increase in the CNR could be detected for 2 D TSE images and in most 2 D GRE images. Hence, they concluded a substantial benefit from the increase of the field strength from 3 T to 7 T for ankle imaging [44]. Current studies have taken 7 T musculoskeletal MRI to the next clinically focused level, enabling sodium imaging in patients after cartilage repair procedures [46, 47] as well as assessment of ultra-structural composition of the Achilles tendon for the detection of early disease [48]. Furthermore, the implementation of 7 T MR spectroscopy (MRS) enables an improved assessment of functional information of healthy and pathological musculoskeletal tissue [49, 50]. Bogner et al. showed a twofold increase of SNR and reduced examination times at 7 T MRS of muscle tissue compared to 3 T [49].

Cardiac imaging

Exploring 7 Tesla MRI beyond neuroradiological and musculoskeletal applications is challenging based on the unavailability of dedicated coil systems. Recent developments in RF coil and shimming techniques have constituted the basis for the application of ultra-high magnetic field strength for anatomical and functional body imaging. With cardiac imaging being one of the first body regions to be investigated beyond brain and musculoskeletal MRI at 7 Tesla, first preliminary results could demonstrate the feasibility and the successful overcoming of technical challenges [51 – 55].

Snyder et al. were one of the first to investigate human cardiac imaging at 7 T [54]. Anatomic and functional images were ac-

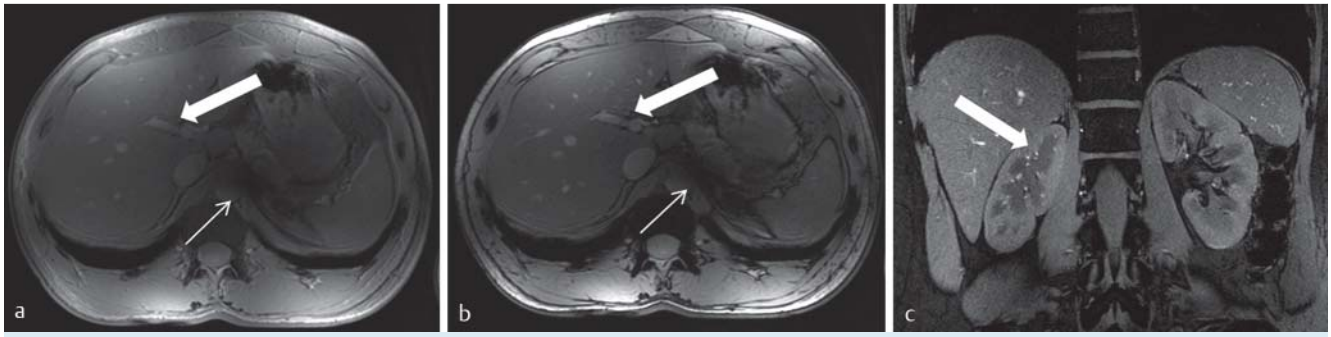

Fig. 5 Non-enhanced T1-weighted 2 D FLASH MRI of the abdomen at 1.5 T **a**, 3 T **b** and 7 T **c** demonstrating high-quality abdominal MRI at all three field strengths and the improved delineation of vessel structures at 7 Tesla due to an inherently hyperintense vessel signal **c**.

Abb. 5 Native T1-gewichtete 2-D-FLASH-Bildgebung bei 1,5 T **a**, 3 T **b** und 7 T **c** zeigt eine hochwertige Darstellung der parenchymatösen Organe bei allen drei Feldstärken und eine hochwertige Darstellung der nativen Gefäßstrombahn bei 7 Tesla aufgrund eines nativ hyperintensen Gefäßsignals **c**. 7 tesla In- **a** und opposed **b** Phase-Bildgebung sowie native 2-D-FLASH-Bildgebung weisen ein homogen hyperintenses Gefäßsignal der abdominellen Gefäßstrombahn auf (breite Pfeile **a** – **c**). Nach der Applikation eines CP2 +-Shim-Modes zeigen sich periaortal residuelle B1-Inhomogenitätsartefakte (dünner Pfeil **a**, **b**).

quired with an eight-channel transmission line (TEM) array, applying local B1 shimming. Their preliminary results of short-axis, four-chamber FLASH cines as well as short-axis TSE images demonstrated the feasibility of in vivo human cardiac imaging at 7 T [54] and built the basis for further dedicated imaging trials [51, 54, 56]. Dieringer et al. recently demonstrated their results on a dedicated 4-channel transmit/receive surface coil suitable for the acquisition of 2 D FLASH cine sequences. Thus, functional cardiac imaging as well as assessment of minor anatomic structures such as the pericardium, valves and trabeculae was successfully performed [51]. Following further coil design developments, Winter et al. investigated the diagnostic ability of three different coil concepts for cardiac MRI, including 4, 8 and 16-channel transmit/receive RF coil configurations. Their study results revealed improved image quality and parallel imaging performance, yet no impact on the accuracy of cardiac chamber quantification could be detected [56].

Abdominal imaging

After the successful demonstration of the feasibility of circumscribed anatomical regions as in cardiac MRI, the scientific focus has shifted towards the investigation of cross-sectional areas as in abdominal MR imaging. Adequate RF shimming is one of the most evident challenges for 7 T abdominal MRI. First imaging results in abdominal imaging using a custom-built 8-channel transmit/receive array with a dedicated add-on RF shimming system were demonstrated by Bitz et al. and Umutlu et al. [24, 25, 27, 57] (**Fig. 5**). To mitigate the restraints based on the reduction of the Larmor wavelength and consecutive destructive B1 interference within the imaged FOV, an add-on RF shimming system was integrated on the small signal side of the MR system. Hardware and software modifications allowed for splitting of the excitation signal of the conventional single-channel system into 8 independent channels. Hence, the application of optimized sets of amplitude and phase shifts to achieve uniform excitation of dedicated body regions becomes possible [57]. The successful clinical implementation of this add-on system has been demonstrated in various abdominal trials [24, 25, 27] (**Fig. 6**).

First feasibility trials in non-enhanced as well as contrast-enhanced kidney and liver MRI revealed considerable differences for T1 and T2-weighted MRI [24, 25, 27]. While T1-weighted images could be obtained with high spatiotemporal resolution yielding high-quality assessment of anatomical details, T2-weighted MRI remained strictly limited due to different challenges. One challenge is posed by residual B1 inhomogeneities, impeding the generation of clean refocusing pulses needed for high-quality T2 TSE imaging [24, 25, 27]. Aside from further improvement of dedicated shimming techniques, one solution to reduce residual B1 inhomogeneities may lie in the application of a dedicated imaging technique named “TIAMO” as introduced by Orzada et al. [28, 29]. Another restriction is the strong increase of energy deposition at 7 Tesla. The associated SAR restrictions particularly hamper the acquisition of RF intense TSE sequences. To better surmount the SAR increase, parallel imaging and a variable flip angle technique can be applied. Nevertheless, the solution attempts have remained insufficient so far [23, 24, 26]. Based on the limitations of current techniques, the impairment of T2-weighted MRI in 7 Tesla abdominal imaging precludes the clinical application of ultra-high-field abdominal MRI for the assessment of the biliary duct system at the moment. As MRCP (magnetic resonance cholangiopancreaticography) imaging is an inevitable part of liver diagnostics, Fischer et al. recently demonstrated their first attempt in performing contrast-enhanced ultra-high-field imaging of the biliary tract using a biliary secreted contrast agent (Gd-EOB-DTPA, Primovist®, Bayer Healthcare) [58]. Their results showed a first successful attempt at contrast-enhanced 7 T bile duct imaging, yielding equivalent imaging results of the central duct segment in comparison to 3 T MRCP imaging [58]. Nevertheless, their results remain preliminary and inferior to 3 Tesla contrast-enhanced biliary imaging based on known restraints in terms of residual B1 field inhomogeneities and inferior coil concepts at an ultra-high-field strength [24, 25, 27].

Demonstrating the general feasibility and strong limitations of ultra-high field abdominal MRI, 7 Tesla T2-weighted MRI as well as bile duct imaging currently remains inferior to 3 Tesla MRI. Further optimization of RF technology and dedicated coil concepts are expected to better cope with current limitations and increase the diagnostic value of ultra-high field abdominal MRI.

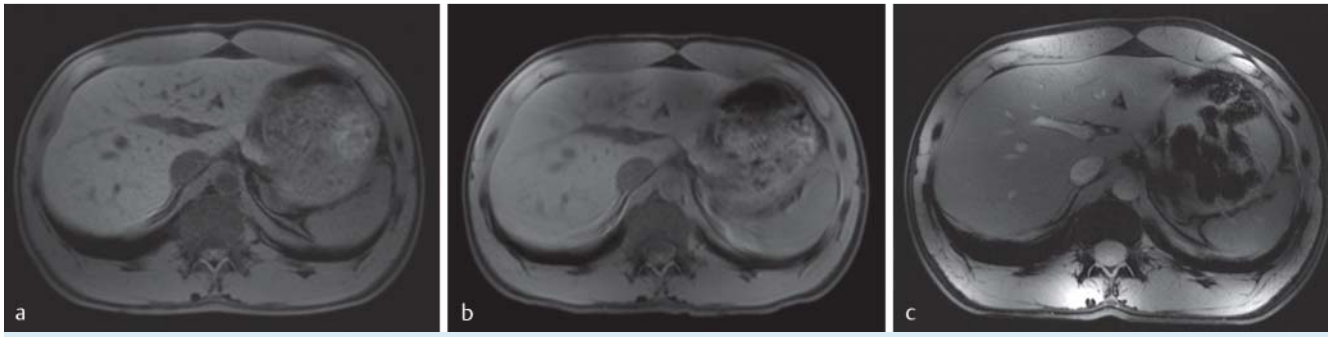

Fig. 6 Non-enhanced T1-weighted 2 D FLASH MRI of the abdomen at 1.5 T **a**, 3 T **b** and 7 T **c** demonstrating high-quality abdominal MRI at all three field strengths and the improved delineation of vessel structures at 7 Tesla due to an inherently hyperintense vessel signal **c**.

Abb. 6 Native T1 gewichtete 2 D FLASH Bildgebung bei 1,5 T **a**, 3 T **b** und 7 T **c** zeigt eine hochwertige Darstellung der parenchymatösen Organe bei allen drei Feldstärken und eine hochwertige Darstellung der nativen Gefäßstrombahn bei 7 Tesla aufgrund eines nativ hyperintensen Gefäßsignals **c**.

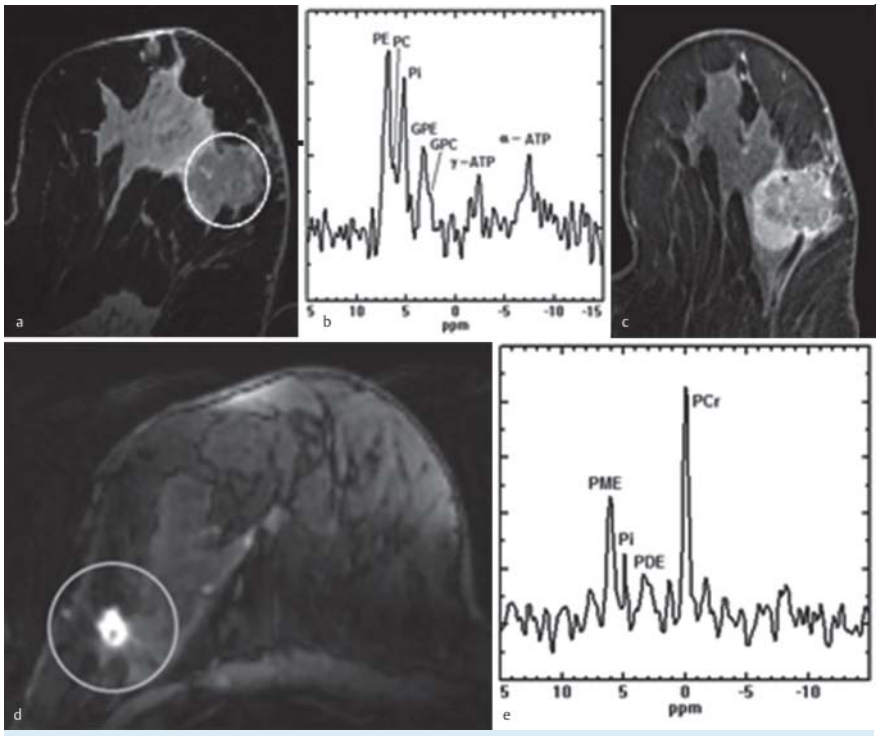

Fig. 7 MR imaging and 31P MR spectroscopy in breast cancer. Top row: invasive ductal carcinoma with 3.2 cm diameter. **a** shows a 7 Tesla T1-weighted image, obtained as described in [59], with the tumor mass encircled, showing good fat suppression and intrinsic contrast without contrast agents. **b** shows corresponding 31P MR spectrum of a Hamming weighted voxel containing the tumor mass showing enhanced intensities of the phosphomonoesters phosphoethanol-amine (PE) and phosphocholine (PC) as compared to the phosphodiesters glycero-phosphoethanolamine (GPE) and glycerophosphocholine (GPC). **c** shows correlating 3 Tesla T1-weighted image after the administration of gadolinium-based contrast agent. Bottom row: ductulolobular carcinoma with 0.9 cm diameter. **a** shows 7 tesla contrast enhanced image showing the very high contrast available at 7 T highlighting tumor mass;. **b** demonstrates corresponding 31P spectrum of a Hamming weighted voxel containing the tumor mass, showing enhanced phosphomonoester (PME) intensity as compared to the phosphodiester

Breast imaging

Several research groups have also investigated the feasibility of 7 Tesla breast MRI and MR spectroscopy. Umutlu et al. demonstrated the feasibility of dynamic contrast-enhanced breast MR imaging at 7 Tesla, enrolling a total of 15 subjects, including 5 patients [59]. Contrast-enhanced T1w MRI could be performed at high spatial resolution, allowing for high-quality assessment of anatomical and pathological structures [59]. Korteweg et al. recently published an intraindividual comparison trial of 3 T and 7 T breast MRI in healthy subjects and breast cancer patients under neoadjuvant chemotherapy (NAC) [60]. The image quality of the unilateral high-resolution scans was rated overall good to excellent by the majority, allowing for improved detection of anatomic details at 7 T. Furthermore, changes in tumor apparent diffusion coefficient values and choline levels indicated positive functional tumor response, corresponding to morphologic tumor size reduction under therapy. Their results demonstrated a 5.7-fold increase in intrinsic SNR in the center of the breast at 7 T compared to 3 T. This strong gain in SNR is probably attributable to a combination of the increase of the magnetic field strength as well as optimization of the applied RF coils at 7 T. The modifications of the RF coil at 7 T include a change in alignment from parallel (at 3 T) to orthogonal (at 7 T) and a +/- 45° angle with respect to the breast instead of a 0° angle at 3 T. This allows for a reduction of the relative distance from the conductors to the breasts at 7 T, enabling a more efficient filling factor of the coil [60]. The successful assessment of biomarkers for breast tumor metabolism at 7 T was also confirmed in further studies on ultra-high-field breast MRS [61, 62] (**Fig. 7**). Wijnen et al. and Klomp et al. investigated 31P (Phosphorus-31) MRS for the in-vivo detection and quantification of total choline compounds as well as levels of further biologic markers. They could show altered levels in patients with breast cancer and modulations under neoadjuvant therapy [61, 62]. Hence, these biomarkers may bear the potential for the noninvasive assessment of prognostic and predictive biomarkers in breast cancer treatment. Nevertheless, dedicated bilateral breast coils constitute a prerequisite for mor-

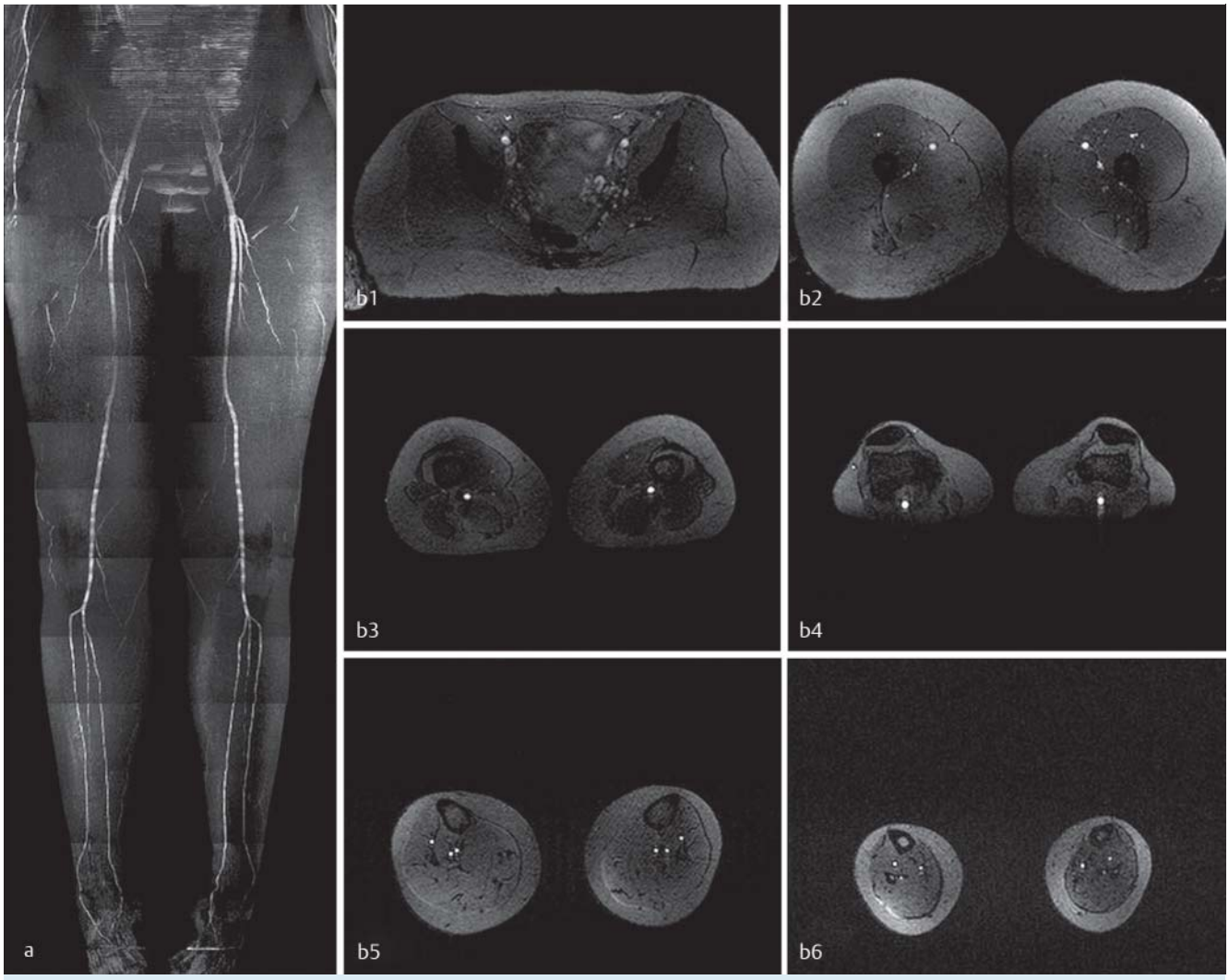

Fig. 8 **a** shows 7 Tesla maximum intensity projection image of non-enhanced T1-weighted 2 D FLASH MRI, covering the arterial vasculature from pelvis to feet **b1 – 6**. Due to effective saturation pulses the signal of surrounding background and venous vasculature could be successfully suppressed [70] (Courtesy of Dr. A. Fischer, Department of Diagnostic and Interventional Radiology and Neuroradiology, University Hospital Essen, Germany).

Abb. 8 **a** zeigt eine 7 Tesla Maximum-Intensity-Projektionsbildgebung einer nativen T1-gewichteten 2-D-FLASH-Bildgebung der arteriellen Becken-Bein-Strombahn. Mit Hilfe effektiver Sättigungspulse konnten das Signal von umgebendem Hintergrund und venöser Gefäße erfolgreich supprimiert werden.

phologic breast MR diagnostics. Therefore, the clinical application of 7 T breast imaging remains restricted.

Pelvis imaging

To date, investigations on prostate MRI at 7 T have focused on proton MR spectroscopic imaging, apart from mere anatomical imaging. Klomp et al. demonstrated the successful detection of resonances of spins of potential tumor markers like creatine and choline [63]. They applied an endorectal transceiver coil system and a pulse sequence with slice selective adiabatic refocusing pulses [63]. Recent publications have mainly focused on the optimization of coil systems for ultra-high-field prostate imaging, as deeply localized organs are known to be challenging with respect to spin excitation and signal reception [64, 65]. Van den Bergen et al. proposed the application of a microstrip array for structural prostate imaging and an endorectal coil for spectroscopy for a full anatomical and functional prostate examination at 7 T [65]. Ipek et al. recently published their results on two different radiative antenna designs employing relative permittivities of 37 and 90 for the antenna substrate. Comparisons of their transmit and receive performance with regard to traditional surface microstrip coils revealed an approximately twofold gain in transmit/receive efficiencies. The antenna was superior with a relative permittivity of 37 based on its minimal RF tissue heating and maximum RF signal depth penetration [64].

While ultra-high-field imaging of the male pelvis in terms of prostate imaging has been well established within the last few years, results on female pelvis MRI remain preliminary. Initial results on female pelvis MRI demonstrated its general feasibility and, comparable to initial results on abdominal MRI, considerable differences in T1 and T2-weighted imaging, currently precluding a potentially clinical application [28].

MR angiography

MR angiography (MRA) is an imaging technique that strongly profits from the increase of the magnetic field strength as demonstrated in 3 T MRA trials. Thus, improved assessment of anatomical and pathological details can be achieved based on increased spatial and temporal resolution [66]. Another beneficial fact is the prolongation of the T1 times of surrounding stationary tissue in comparison to blood. This results in an improved vessel-to-background contrast [6, 7].

Starting out with imaging of the intracranial arteries, 7 T MR angiography has currently expanded to imaging of the extracranial carotid arteries [67], coronary arteries [68] as well as renal arteries [69, 70]. Umutlu et al. and Metzger et al. demonstrated the feasibility of non-enhanced renal MRA at 7 Tesla, performing TOF MRA as well as 2 D and 3 D FLASH imaging [69, 70]. TOF MRA revealed its diagnostic superiority due to high vessel-to-background contrast compared to FLASH imaging [70]. The application of non-enhanced ultra-high-field MRA has recently also been successfully expanded to imaging of the vessels of the lower extremities [71] (**Fig. 8**).

This method may be beneficial in patients with impaired renal function. Nevertheless, the inherently hyperintense signal also has the potential to impair the efficient applicability of intravenous gadolinium administration for contrast-enhanced 7 T MRA, in terms of hindered subtraction imaging. Initial results on first-pass renal MRA at 7 Tesla have recently been demonstrated, revealing general feasibility of contrast-enhanced renal MRA with improved vessel delineation after the application of gadolinium [72].

Conclusion

In summary, we can conclude that 7 Tesla MR imaging has come a long way since its first clinical applications in 2006, expanding the application range from brain and musculoskeletal imaging to whole-body applications including contrast-enhanced data sets. The scientific focus has transitioned from structural investigations to the assessment of functional parameters within time. Imaging of circumscribed anatomical regions without the obligation of breath-hold imaging as in brain and musculoskeletal MRI has been well established in scientific and clinical trials. However, body imaging at 7 T is still in the initial stages of trying to utilize the opportunities and overcome the challenges of ultra-high magnetic field strength. The focus of future studies will be the further optimization of dedicated coil and shimming techniques as well as investigations of the diagnostic ability of 7 Tesla imaging in the case of patient studies.

References

1 *Robitaille PML, Abduljalil AM, Kangarlu A et al.* Human magnetic resonance imaging at 8 T. NMR in Biomedicine 1998; 11: 263 – 265
2 *Kangarlu A, Abduljalil AM, PM R.* T1- and T2-weighted imaging at 8 Tesla. J Comput Assist Tomogr 1999; 23: 875 – 878
3 *Kangarlu A, Abduljalil AM, Schwarzbauer C et al.* Human rapid acquisition with relaxation enhancement imaging at 8 T without specific absorption rate violation. MAGMA 1999; 9: 81 – 84
4 *Norris DG, Kangarlu A, Schwarzbauer C et al.* MDEFT imaging of the human brain at 8 T. Magma 1999; 9: 92 – 96
5 *Moser E, Stahlberg F, Ladd ME et al.* 7-T MR—from research to clinical applications? NMR in Biomedicine 2012; 25: 695 – 716
6 *Barth MM, Smith MP, Pedrosa I et al.* Body MR Imaging at 3.0 T: Understanding the Opportunities and Challenges. Radiographics 2007; 27: 1445 – 1462
7 *Chang KJ, Kamel IR, Macura KJ et al.* 3.0-T MR Imaging of the Abdomen: Comparison with 1.5 T1. Radiographics 2008; 28: 1983 – 1998
8 *Kuhl CK, Träber F, Schild HH.* Whole-Body High-Field-Strength (3.0-T) MR Imaging in Clinical Practice Part I. Technical Considerations and Clinical Applications1. Radiology 2008; 246: 675 – 696
9 *Kollia K, Maderwald S, Putzki N et al.* First Clinical Study on Ultra-High-Field MR Imaging in Patients with Multiple Sclerosis: Comparison of 1.5T and 7T. AJNR Am J Neuroradiol 2009; 4: 699 – 702
10 *Moenninghoff C, Maderwald S, Theysohn JM et al.* Evaluation of intracranial aneurysms with 7 T versus 1.5 T time-of-flight MR angiography – initial experience. Beurteilung von intrakraniellen Hirnarterienaneurysmen mit 7 Tesla versus 1,5 Tesla-Time-of-Flight-MR-Angiografie erste Erfahrungen. Fortschr Röntgenstr 2009; 181: 16 – 23
11 *Moenninghoff C, Maderwald S, Theysohn J et al.* Imaging of adult astrocytic brain tumours with 7 T MRI: preliminary results. European Radiology 20: 704 – 713
12 *Moenninghoff C, Maderwald S, Theysohn JM et al.* Imaging of Brain Metastases of Bronchial Carcinomas with 7T MRI "Initial Results" Fortschr Röntgenstr 182: 764 – 772
13 *Mönninghoff C, Maderwald S, Wanke I.* Pre-Interventional Assessment of a Vertebrobasilar Aneurysm with 7 Tesla Time-of-Flight MR Angiography. Fortschr Röntgenstr 2009; 181: 266 – 268
14 *Theysohn JM, Kraff O, Maderwald S et al.* 7 tesla MRI of microbleeds and white matter lesions as seen in vascular dementia. Journal of Magnetic Resonance Imaging 33: 782 – 791
15 *Bernstein MA, Huston JIII, Ward H.* Imaging artifacts at 3.0T. Journal of Magnetic Resonance Imaging 2006; 24: 735 – 746
16 *Boll DT, Merkle EM.* Imaging at Higher Magnetic Fields: 3 T Versus 1.5 T. Magnetic resonance imaging clinics of North America 2010; 18: 549 – 564
17 *Martin DR, Friel HT, Danrad R et al.* Approach to abdominal imaging at 1.5 Tesla and optimization at 3 Tesla. Magn Reson Imaging Clin N Am 2005; 13: 241 – 254
18 *Merkle EM, Dale MB, EK P.* Abdominal MR Imaging at 3T. Magnetic resonance imaging clinics of North America 2006; 14: 17 – 26
19 *Merkle EM, Dale BM.* Abdominal MRI at 3.0 T: The Basics Revisited. Am J Roentgenol 2006; 186: 1524 – 1532
20 *Elster AD.* Eur Radiol; 1997; 7 (Suppl 5): 276 – 280 Eur Radiol 1997; 21.
21 *de Bazelaire CMJ, Duhamel GD, Rofsky NM et al.* MR Imaging Relaxation Times of Abdominal and Pelvic Tissues Measured in Vivo at 3.0 T: Preliminary Results1. Radiology 2004; 230: 652 – 659
22 *Ladd M.* High-Field-Strength Magnetic Resonance: Potential and Limits. Topics in Magnetic Resonance Imaging 2007; 18: 139 – 152
23 *Wolf S, Diehl D, Gebhardt M et al.* SAR Simulations for High-Field MRI: How Much Detail, Effort, and Accuracy Is Needed? Magnetic Resonance in Medicine 2012; DOI: DOI 10.1002/mrm.24329
24 *Umutlu L, Orzada S, Kinner S et al.* Renal Imaging at 7 Tesla: Preliminary Results. European Radiology 2010; 21: 841 – 849
25 *Umutlu L, Kraff O, Orzada S et al.* Dynamic Contrast-Enhanced Renal MRI at 7 Tesla: Preliminary Results. Invest Radiol 2011; 46: 425 – 433
26 *Kalender W, Quick H.* Recent advances in medical physics. European Radiology 2011; 21: 501 – 504
27 *Umutlu L, Bitz AK, Maderwald S et al.* Contrast-enhanced ultra-high-field liver MRI: A feasibility trial. European Journal of Radiology 2012; 4: e625 – e628
28 *Umutlu L.* Female pelvis MRI at 7T. Proceedings of the 17th Annual Meeting of ISMRM 2011
29 *Orzada S, Johst S, Maderwald S et al.* Mitigation of B1+ inhomogeneity on single-channel transmit systems with TIAMO. Magnetic Resonance in Medicine 2012; DOI: doi: 10.1002/mrm.24453
30 *Orzada S, Maderwald S, Poser BA et al.* RF excitation using time interleaved acquisition of modes (TIAMO) to address B1 inhomogeneity in high-field MRI. Magnetic Resonance in Medicine 64: 327 – 333
31 *Maderwald S, Ladd S, Gizewski E et al.* To TOF or not to TOF: strategies for non-contrast-enhanced intracranial MRA at 7 T. Magnetic Resonance Materials in Physics, Biology and Medicine 2008; 21: 159 – 167
32 *Zwanenburg JJ, Hendrikse J, Takahara T et al.* MR angiography of the cerebral perforating arteries with magnetization prepared anatomical reference at 7T: comparison with time-of-flight. Journal of Magnetic Resonance Imaging 2008; 28: 1519 – 1526

33 *Grinstead JW*, *Rooney W*, *Laub G*. The Origins of Bright Blood MPRAGE at 7 Tesla and a Simultaneous Method for T1 Imaging and Non-Contrast MRA. Proc Intl Soc Mag Reson Med 2010; 18: 1429
34 *Willinek WA*, *Born M*, *Simon B et al.* Time-of-Flight MR Angiography: Comparison of 3.0-T Imaging and 1.5-T Imaging–Initial Experience. Radiology 2003; 229: 913 – 920
35 *Ty BaeK*, *Park S-H*, *Moon C-H et al.* Dual-echo arteriovenography imaging with 7T MRI. Journal of Magnetic Resonance Imaging 2010; 31: 255 – 261
36 *Heverhagen JT*, *Bourekas E*, *Sammet S et al.* Time-of-flight magnetic resonance angiography at 7 Tesla. Invest Radiol 2008; 43: 568 – 573
37 *Stamm AC*, *Wright CL*, *Knopp MV et al.* Phase contrast and time-of-flight magnetic resonance angiography of the intracerebral arteries at 1.5, 3 and 7 T. Magnetic Resonance Imaging Epub ahead of print 2012. DOI: 10.1016
38 *Yacoub E*, *Shmuel A*, *Pfeuffer J et al.* Imaging brain function in humans at 7 Tesla. Magn Reson Med 2001; 45: 588 – 594
39 *van der Zwaag W*, *Marques JP*, *Kober T et al.* Temporal SNR characteristics in segmented 3D-EPI at 7T. Magn Reson Med 2011; 67: 344 – 352
40 *Fleysher L*, *Oesingmann N*, *Brown R et al.* Noninvasive quantification of intracellular sodium in human brain using ultrahigh-field MRI. NMR Biomed 2012; DOI: doi: 10.1002/nbm.2813
41 *Madai VI*, *von Samson-Himmelstjerna FC*, *Bauer M et al.* Ultrahigh-Field MRI in Human Ischemic Stroke – a 7 Tesla Study. PLoS ONE 2012; 7: e37631
42 *Banerjee S*, *Krug R*, *Carballido-Gamio J et al.* Rapid in vivo musculoskeletal MR with parallel imaging at 7T. Magnetic Resonance in Medicine 2008; 59: 655 – 660
43 *Kraff O*, *Theysohn JM*, *Maderwald S et al.* MRI of the Knee at 7.0 Tesla. MRT des Kniegelenks bei 7,0 Tesla 2007; 179: 1231 – 1235
44 *Juras V*, *Welsch G*, *Bär P et al.* Comparison of 3T and 7T MRI clinical sequences for ankle imaging. European Journal of Radiology 2012; 8: 1846 – 1850
45 *Welsch G*, *Juras V*, *Szomolanyi P et al.* Magnetic resonance imaging of the knee at 3 and 7 Tesla: a comparison using dedicated multi-channel coils and optimised 2D and 3D protocols. European Radiology 2012; 9: 1852 – 1859
46 *Madelin G*, *Babb JS*, *Xia D et al.* Reproducibility and repeatability of quantitative sodium magnetic resonance imaging in vivo in articular cartilage at 3 T and 7 T. Magnetic Resonance in Medicine 2012; 3: 841 – 849
47 *Madelin G*, *Chang G*, *Otazo R et al.* Compressed sensing sodium MRI of cartilage at 7T: Preliminary study. Journal of Magnetic Resonance 2012; 214: 360 – 365
48 *Juras V*, *Zbýň Š*, *Pressl C et al.* Sodium MR Imaging of Achilles Tendinopathy at 7 T: Preliminary Results. Radiology 2012; 262: 199 – 205
49 *Bogner W*, *Chmelik M*, *Schmid AI et al.* Assessment of 31P relaxation times in the human calf muscle: A comparison between 3 T and 7 T in vivo. Magnetic Resonance in Medicine 2009; 62: 574 – 582
50 *Trattnig S*, *Zbýň Š*, *Schmitt B et al.* Advanced MR methods at ultra-high field (7 Tesla) for clinical musculoskeletal applications. European Radiology 2012, Epub ahead of print.
51 *Dieringer MA*, *Renz W*, *Lindel T et al.* Design and application of a four-channel transmit/receive surface coil for functional cardiac imaging at 7T. Journal of Magnetic Resonance Imaging 2011; 33: 736 – 741
52 *Hezel F*, *Thalhammer C*, *Waiczies S et al.* High spatial resolution and temporally resolved t(2) (*) mapping of normal human myocardium at 7.0 tesla: an ultrahigh field magnetic resonance feasibility study. PLoS One 2012; 7: e52324 . DOI: 10.1371 /journal.pone.0052324
53 *von Knobelsdorff-Brenkenhoff F*, *Frauenrath T*, *Prothmann M et al.* Cardiac chamber quantification using magnetic resonance imaging at 7 Tesla—a pilot study. European Radiology 2010; 20: 2844 – 2852
54 *Snyder CJ*, *DelaBarre L*, *Metzger GJ et al.* Initial results of cardiac imaging at 7 tesla. Magnetic Resonance in Medicine 2009; 61: 517 – 524
55 *Suttie JJ*, *DelaBarre L*, *Pitcher A et al.* 7 Tesla (T) human cardiovascular magnetic resonance imaging using FLASH and SSFP to assess cardiac function: validation against 1.5 T and 3 T. NMR in Biomedicine 2012; 25: 27 – 34
56 *Winter L*, *Kellman P*, *Renz W et al.* Comparison of three multichannel transmit/receive radiofrequency coil configurations for anatomic and functional cardiac MRI at 7.0T: implications for clinical imaging. European Radiology 2012; DOI: 10.1007/s00330-012-2487-1
57 *Bitz A*, *Brote I*, *Orzada S et al.* Am 8-channel add-on RF shimming system for whole-body 7 Tesla MRI including real-time SAR monitoring. Proceedings of the 17th Annual Meeting of ISMRM, HI, USA 2009, (Abstract 4767)
58 *Fischer A*, *Kraff O*, *Umutlu L et al.* Ultra high-field imaging of the biliary tract at 7 Tesla: initial results of Primovist® enhanced MRCP. Proceedings of the 18th Annual Meeting of ISMRM 2012
59 *Umutlu L*, *Maderwald S*, *Kraff O et al.* Dynamic Contrast-Enhanced Breast MRI at 7 Tesla Utilizing a Single-loop Coil: A Feasibility Trial. Academic Radiology 17: 1050 – 1056
60 *Korteweg MA*, *Veldhuis WB*, *Visser F et al.* Feasibility of 7 Tesla breast magnetic resonance imaging determination of intrinsic sensitivity and high-resolution magnetic resonance imaging, diffusion-weighted imaging, and (1)H-magnetic resonance spectroscopy of breast cancer patients receiving neoadjuvant therapy. Investigative Radiology 2011; 46: 370 – 376
61 *Klomp DWJ*, *van de Bank BL*, *Raaijmakers A et al.* 31P MRSI and 1H MRS at 7 T: initial results in human breast cancer. NMR in Biomedicine 2011; 24: 1337 – 1342
62 *Wijnen JP*, *van der Kemp WJM*, *Luttje MP et al.* Quantitative 31P magnetic resonance spectroscopy of the human breast at 7 T. Magnetic Resonance in Medicine 2012; 68: 339 – 348
63 *Klomp DWJ*, *Bitz AK*, *Heerschap A et al.* Proton spectroscopic imaging of the human prostate at 7 T. NMR in Biomedicine 2009; 22: 495 – 501
64 *Ipek O*, *Raaijmakers AJ*, *Klomp DW et al.* Characterization of transceive surface element designs for 7 tesla magnetic resonance imaging of the prostate: radiative antenna and microstrip. Phys Med Biol 2011; 57: 343 – 355
65 *van den Bergen B*, *Klomp DWJ*, *Raaijmakers AJE et al.* Uniform prostate imaging and spectroscopy at 7 T: comparison between a microstrip array and an endorectal coil. NMR in Biomedicine 2011; 24: 358 – 365
66 *Lanzman RS*, *Kröpil P*, *Schmitt P et al.* Nonenhanced Free-Breathing ECG-Gated Steady-State Free Precession 3D MR Angiography of the Renal Arteries: Comparison Between 1.5 T and 3 T. American Journal of Roentgenology 2010; 194: 794 – 798
67 *Kraff O*, *Bitz AK*, *Breyer T et al.* A Transmit/Receive Radiofrequency Array for Imaging the Carotid Arteries at 7 Tesla: Coil Design and First In Vivo Results. Investigative Radiology 2011 46: 246 – 254
68 *van Elderen SGC*, *Versluis MJ*, *Webb AG et al.* Initial results on in vivo human coronary MR angiography at 7 T. Magnetic Resonance in Medicine 2009; 62: 1379
69 *Metzger GJ*, *Auerbach EJ*, *Akgun C et al.* Dynamically applied B1+ shimming solutions for non-contrast enhanced renal angiography at 7.0 tesla. Magnetic Resonance in Medicine 2012: n/a – n/a
70 *Umutlu L*, *Maderwald S*, *Kraff O et al.* New look at renal vasculature: 7 tesla nonenhanced T1-weighted FLASH imaging. Journal of Magnetic Resonance Imaging 2012; 36: 714 – 721
71 *Fischer A*, *Maderwald S*, *Orzada S et al.* Nonenhanced magnetic resonance angiography of the lower extremity vessels at 7 tesla: Initial experience. Invest. Radiol 2013, [Epub ahead of print]
72 *Umutlu L*, *Maderwald S*, *Kinner S et al.* 7 Tesla Abdominal Vessel Imaging: Do We Really Need Gadolinium? RSNA Radiology: S 293 2011